5th International/11th Construction Specialty Conference
5e International/11e Conférence spécialisée sur la construction

Vancouver, British Columbia
June 8 to June 10, 2015 / *8 juin au 10 juin 2015*

INFRASTRUCTURE CONDITION ASSESSMENT BASED ON LOW-COST HYPER-SPATIAL RESOLUTION MULTISPECTRAL DIGITAL AERIAL PHOTOGRAPHY

Su Zhang[1, 2, 3], Susan M. Bogus[1], and Christopher D. Lippitt[2]
[1] Department of Civil Engineering, University of New Mexico, United States
[2] Department of Geography and Environmental Studies, University of New Mexico, United States
[3] suzhang@unm.edu

Abstract: Infrastructure condition information is critical for effective asset management. Infrastructure managers are tasked with regularly assessing asset conditions to make effective maintenance, repair, and rehabilitation decisions. Currently there are two types of methods broadly adopted for infrastructure condition assessment: on-site evaluation methods and airplane-based observation methods. On-site evaluation methods are expensive, labor-intensive, time-consuming, potentially dangerous to inspectors, inconsistent, and requiring specialized staff on a regular basis. Airplane-based observation methods can provide reliable overall condition information for ground infrastructure assets such as roadways, bridges, dams, or buildings, but the spatial resolutions of 0.075-meter (3-inch) to 1-meter are insufficient to examine detailed asset conditions such as individual cracks on a pavement surface or on a bridge. Using roadway pavement assets as an example, this research explored the utility of hyper-spatial resolution (3-millimeter) multispectral digital aerial photography acquired from a low-altitude unmanned remote sensing system to permit characterization of detailed surface distress conditions. With the help of orthogonal regression analysis, detailed pavement surface distress rates manually estimated from hyper-spatial resolution multispectral digital aerial photography were compared to reference pavement distress rates manually collected on the ground. The results show that the hyper-high spatial resolution imaging techniques provide detailed and reliable data suitable for informing infrastructure system management decisions. These results open the way for the future application of low-cost hyper-spatial resolution digital aerial photography for automated assessment of detailed infrastructure system condition.

1 INTRODUCTION

Infrastructure condition information is critical for effective infrastructure system management (Zhang and Bogus 2014). Decisions involving maintenance, repair, and rehabilitation of infrastructure systems require accurate and current information describing the conditions of these systems and their components (Maser 2005). This information is required not only to characterize current conditions but also to project future performance and remaining life (Maser 2005). Therefore, infrastructure managers are tasked with regularly assessing asset conditions to make effective maintenance, repair, and rehabilitation decisions.

Currently, infrastructure management agencies use either on-site evaluation or airplane-based observation methods for infrastructure condition assessment. On-site evaluation methods are labor-intensive, time-consuming, and potentially dangerous to inspectors (Maser 2005). Airplane-based observation methods can provide reliable overall condition information for ground infrastructure assets

such as roadways, bridges, or buildings (Zhang and Bogus 2014), but the spatial resolutions of 0.075-meter (3-inch) to 1-meter are insufficient to examine detailed asset conditions such as individual cracks on a pavement surface or on a bridge. In recent years, unmanned remote sensing systems (URSS) have emerged as an important platform for hyper-spatial resolution aerial data collection. URSS can fly lower to the ground than traditional airplanes, and thus allow for more detailed data to be collected without specially-designed, cost prohibitive sensors (e.g. LiDAR). Using roadway pavement assets as an example, this research explored the utility of hyper-spatial resolution (3-millimeter) multispectral digital aerial photography (H-DAP) acquired from a low-altitude URSS, in this case a tethered weather balloon, to permit characterization of detailed surface distress conditions. Detailed pavement surface distress rates manually estimated from H-DAP were compared to reference distress rates manually collected on the ground to assess the feasibility and potential utility of automated approaches.

2 BACKGROUND

The ability to assess the condition of infrastructure systems (e.g. roads and bridges) rapidly and accurately is critical to making decisions within any infrastructure management systems (Maser 1988; Karaa 1989). Infrastructure condition data are collected and used by infrastructure management agencies to determine the serviceability of infrastructure systems and to help make decisions on the distribution of limited resources for maintenance, repair, and rehabilitation.

Traditionally, infrastructure assessment is performed with “boots on the ground” by having experts visually inspect the condition of infrastructure systems with subjective judgment (Aktan et al. 1996) or by using vehicle-mounted electronic sensors to automatically detect the infrastructure conditions (Hudson and Uddin 1987). This type of assessment method is classified as on-site evaluation and still broadly used by infrastructure system management agencies. In recent history, one might still remember structural engineers scaling the Washington Monument in Washington, D.C. after the 2011 earthquake to determine the structural integrity of the monument (Figure 1). On-site condition assessment can collect detailed infrastructure condition data. However, on-site methods are expensive, labor-intensive, time-consuming, potentially dangerous to inspectors, requiring specialized staff on a regular basis, and data collected by different inspectors can exhibit a high degree of variability (Maser 2005; Bogus et al. 2010).

Figure 1: Post-earthquake assessment of Washington Monument (Source: NPS.gov)

Another method to assess infrastructure conditions is using remote evaluation methods. This technology is typically deployed on airplanes that fly over infrastructure systems. This type of assessment method is classified as airplane-based observation evaluation and is becoming more and more popular (Jensen and Cowen 1999). The resulting images (Figure 2), which typically have spatial resolutions ranging from 0.075-meter (3-inch) to 1-meter, can be used to evaluate the overall condition of infrastructure systems rapidly and inexpensively (Zhang and Bogus 2014). There are limitations, however, on the spatial resolution of these images which can limit the ability to detect and assess small defects, such as cracks on a pavement surface or on a bridge (Guo 2010).

The intellectual significance of this research is that it addresses the limitations inherent in both the “boots on the ground” method and the aerial data collected from airplane-based technology by using a novel middle ground approach of data collection for detailed infrastructure condition assessment. The proposed

methods uses an unmanned airborne system (UAS), which can fly lower to the ground than traditional airplanes, and thus allow for more detailed infrastructure condition data to be collected without specially designed, cost prohibitive sensors. The improved detail associated with the data holds the potential to provide much better condition assessment of infrastructure systems at dramatically reduced cost when compared to on-site (i.e. manual methods or automatic methods) approaches.

Figure 2: Routinely available airplane-based observation images for infrastructure condition assessment; this image has a spatial resolution of 0.1524-meter (6-inch).

In recent years, UAS have emerged as an important platform for collection of hyper-spatial resolution aerial data (i.e., sub-centimeter ground sampling distances) – a trend that is all but certain to continue. For now, due to a wide variety of regulatory and safety concerns, the legal use of UAS is severely restricted in the United States. In anticipation of an established regulatory environment and availability of UAS for routine infrastructure condition assessment, this research used a tethered helium weather balloon system to simulate the collection of hyper-spatial resolution aerial image data from untethered UAS. The process of measuring spatial properties from aerial photography or images is referred to as "photogrammetry". Aerial triangulation (AT) is the basic photogrammetric method for analyzing aerial images to determine X, Y, and Z ground coordinates of individual points based on measures take from a series of overlapping aerial photographs (Zomrawi et al. 2013). AT traditionally requires the identification of thousands of control points linking images to one another and to a reference dataset to enable least squares estimation of the optimal triangulation model. New computation approaches (e.g., structure-from-motion, graphic processing unit based image processing) have enabled automation of traditional AT to permit routine estimation of 3-dimensional surface structure and subsequent orthocorrection of large datasets at approximately the spatial resolution of the input images (Zhang et al. 2011; Zomrawi et al. 2013). When coupled with hyper-spatial resolution image data such as that collected by low altitude UAS, this technology holds the potential to permit the estimation of horizontal and vertical measurements at sub-centimeter scales (Zhang et al. 2011), and ultimately, the detection and assessment of infrastructure damages at finer scales than has traditionally been possible by airborne survey.

Hyper-spatial resolution aerial data have been used to facilitate research in many fields, such as archaeology, intertidal ecology, marine ecology, zoology, emergency management, vegetation and soil monitoring, and topographic mapping (Scoffin 1982; Aber et al. 1999; Fraser et al. 1999; Guichard et al. 2000; Aber et al. 2001; Sklaver et al. 2006; Wundram and Loffler 2008; Marzolff and Poesen 2009; Smith et al. 2009; Verhoeven 2009). However, previous studies regarding application of H-DAP to detailed infrastructure condition assessment are limited. The only published research on this topic was performed by Chen et al. (2011). This research shows the potential to use H-DAP to evaluate crack-level infrastructure condition, but the assessment ability is limited to inch-level large cracks on bridge pavements because the spatial resolution of the used aerial images is 0.0254-meter (1-inch).

Using roadway flexible pavement (i.e. asphalt concrete) assets as an example, we explore the application of H-DAP to detect and assess detailed infrastructure condition. Key items for evaluating flexible pavement distress were identified from United States Department of Transportation Highway Performance System (HPMS) Field Manual, including rutting (item 50), alligator cracking (item 52), and transverse cracking (item 53). Rutting is an unrecoverable longitudinal surface depression in both wheel paths (Cordova et al. 2009). Alligator cracking is interconnected cracks resembling chicken wire or alligator skin (Cordova et al. 2009). Transverse cracking is cracking that is predominantly perpendicular to the pavement centerline. Transverse cracking is a result of pavement expansion and contraction due to

temperature changes, as well as shrinkage of asphalt binder with aging (Cordova et al. 2009). With AT, it is possible to generate sub-centimeter scale mosaicked orthophotos and digital surface models (DSMs) for standardized evaluation of detailed infrastructure condition, potentially reducing the cost and duration of assessment while improving the comparability of results.

3 METHODOLOGY

Using H-DAP acquired from a low-cost UAS as input, AT was used to generate 3-millimeter spatial resolution mosaicked orthophotos and same spatial resolution DSMs for pavement surfaces. Key metrics (HPMS Field Manual 2010) used to measure flexible pavement distress, including cracking length, cracking area percentage, and rutting depth, were measured from the orthophotos and DSMs and then compared to ground reference data measured manually using standard protocols (Cordova et al. 2009).

3.1 Data Acquisition and Preparation

A low-cost unmanned remote system was developed to simulate the collection of image data from other untethered low-altitude UAS that are now common in the marketplace. This system includes a tethered helium weather balloon with customized rigging. The sensor affixed to the balloon rigging is a small-format Canon digital camera (SX260 HS). This camera has a 12 megapixel detector array collecting in the visible blue, green, and red wavelength via Bayer array sampling, a rugged cased with protected lens, built-in GPS unit, and intervalometer capability. A firmware enhancement application known as the Canon Hack Development Kit (CHDK), was employed to permit more control over the operation of the Canon SX260 HS digital camera, including shutter speed, shutter lag, aperture size, and intervalometer.

Data were collected for ten sites (i.e. road sections) on US Highway 66 and New Mexico Highway 0333 near the City of Albuquerque, NM. Approximately 200 overlapping hyper-spatial resolution aerial images were acquired for each site at about 40 meters above ground level (AGL). The ground area covered by each frame is approximately 20-meter by 15-meter and the ground sampling distance is approximately 2-millimeter. A Real Time Kinematic (RTK) surveying system was used to collect the horizontal and vertical coordinates of the ground control points (GCPs) on the pavement surface with a National Oceanic and Atmospheric Administration (NOAA) Online Positioning User Service (OPUS) reported root mean squared error (RSME) of 0.004-meter horizontally and 0.006-meter vertically. Sixteen GCPs were collected along with detailed photos of each GCP for each site.

A reference data set was collected by a trained two-person crew at each of the preselected data collection sites. Crew members performed manual (i.e., visual) evaluation with safety precautions (e.g. safety training and high visibility garments) based on the standard protocol adopted by the HPMS Field Manual. Both inspectors assessed pavement distresses (rutting, alligator cracking, and transverse cracking) independently and the results are the average value of the two independent evaluations. In accordance with the HPMS Field Manual, rutting and shoving depth was measured for only the rightmost driving lane for both inner and outer wheel paths at three locations along the wheel path within each site and then the depth averaged for each wheel path. The HPMS Field Manual requires reporting the percent area of total alligator cracking to the nearest 5%. In addition, the HPMS Field Manual requires reporting an estimation of relative length in feet per mile (feet/mile) of transverse cracking.

3.2 Aerial Triangulation (AT)

After excluding blurry and oblique images, approximately 150 overlapping hyper-spatial resolution aerial images were used for each site. The commercial software Agisoft was selected as the tool to perform AT as it permitted minimal human intervention at a low cost. Among the sixteen GCPs collected for each site, ten were used to calibrate the AT process while the remaining six were reserved to evaluate the horizontal and vertical accuracy of the orthophotos and DSMs. For each site, millions of control points were identified from the input overlapping images to build a dense cloud, and then a triangulation irregular network (TIN) mesh was generated based on the identified control points. Orthophotos and DSMs were exported as raster datasets in TIFF format at a spatial resolution of 3-millimeter. Orthophotos and DSMs are generated in a single processing routine and are therefore tightly co-registered. Orthophotos were

used to assess the horizontal accuracy while DSMs were used to assess the vertical accuracy. The accuracy assessment results (RMSE) show that the overall horizontal accuracy for all data collection sites is 0.004-meter, while the vertical accuracy is 0.006-meter. The number of overlapping images used and accuracy information for each data collection site is reported in Table 1.

Table 1: Images Frames and Accuracy of Orthophotos and DSMs for Each Site

Site Name	Image Frames	Horizontal Accuracy (in meters)	Vertical Accuracy (in meters)
Site 1	122	0.002	0.006
Site 2	135	0.005	0.004
Site 3	183	0.005	0.003
Site 4	177	0.004	0.009
Site 5	181	0.003	0.007
Site 6	180	0.004	0.006
Site 7	165	0.004	0.004
Site 8	133	0.004	0.006
Site 9	126	0.003	0.005
Site 10	189	0.003	0.004
Overall	1591	0.004	0.006

3.3 Rutting Depth Measurement

In manual evaluation, rutting depth was measured with a wooden bar and a measuring tape. The actual measured points are the lowest points as visually determined by inspectors. DSMs exhibit the modeled 3-dimensional pavement surface. Points and polygons were created on DSMs to simulate the locations of the actual measuring points and wooden bars for rutting depth measurement. The actual measuring points and the locations of the wooden bars are shown in Figure 3.

The minimum scale of the measuring tape used for manual inspection was 0.001-meter. The length and width of the wooden bar is 1.22-meter (48-inch) and 0.02-meter (0.8-inch). With the actual field measured point (as photographed) as the center, two polygons (one on either side of the field measured point) with a size of 0.61-meter (20-inch) by 0.02-meter were created to simulate the location of the wooden bar. Using the polygon as the boundary, the DSM pixels were extracted and the highest measured points were identified to correspond to the field method of rutting depth calculation. Figure 4 illustrates the method used to calculate rutting depth from the DSM.

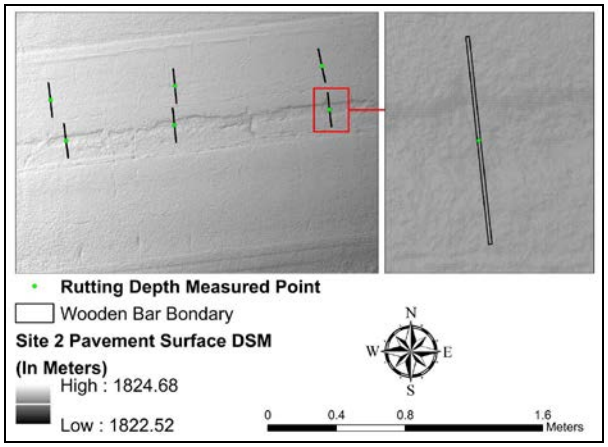

Figure 3: Locations of actual measured points and wooden bars

As shown in Figure 4, we consider the two highest points of the rutting section points A and B and the two measured points of the rutting section Points C and D. The distance from Point C to Point D is the rutting depth. Points A, B, and C will have the same height if the heights of Points A and B are equal. However, under most circumstances the heights of A and B are different. Therefore, a weighted average method was used to estimate the height of Point C:

[1] HC = (HA * DA + HB * DB) / (DA + DB)

[2] RD = HC - HD

In Equation 1, HC represents the height of Point C, while HA and HB represent the heights of Point A and Point B, respectively. DA represents the horizontal distance from Point A to Point D, while DB represents the horizontal distance from Point B to Point D. In Equation 2, RD represents the rutting depth. HA and HB were determined based on the DSMs, while DA and DB were determined based on the orthophotos.

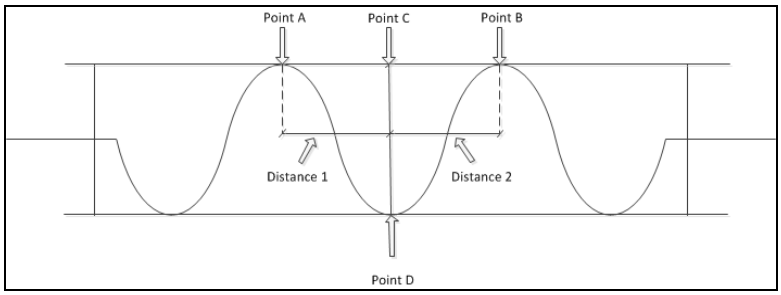

Figure 4: Rutting depth calculation process

3.4 Alligator Cracking Measurement

As required by the HPMS Field Manual, alligator cracking should be reported as the percent of total alligator cracking section area to the nearest 5% at a minimum. In the manual evaluation protocol (Cordova et al. 2009), pavement inspectors pace off the cumulative length of alligator cracking and mark the location of occurrence in 1 or 2 wheel paths. For example, typically the width of the driving lane is 3.66 meters (12 feet), and therefore, for a 1.6 kilometer (1 mile) section, the total area is 5886 square meters (63360 square feet). If the total length of alligator cracking paced off by inspectors is 152 meters (500 feet) in both wheel paths and the width of the evaluated alligator cracking is 0.61 meters (2 feet), the total area of the alligator cracking is 185 square meters (2000 square feet). Therefore, the reported area percentage should be 5 percent (2000/63360 = 3.2 percent which should be rounded up to the nearest 5 percent). In order to simulate the alligator cracking measurement prescribed by the HPMS, polygons were created to represent the whole pavement surface section used for manual evaluation and the boundary of the occurred alligator cracking. The polygon defining the manual evaluation zone was used to calculate the total area while the polygon defining the alligator cracking was used to calculate the total area of alligator cracking, and then the percent of alligator cracking was calculated by comparing the two polygons. The usage of polygons to determine the area percentage is shown in Figure 5. It should be noted that both actual percentage and rounded percentage were calculated for each site, but only rounded percentage was used for the following analyses.

3.5 Transverse Cracking Measurement

According to the HPMS Field Manual, pavement inspectors should count the number of transverse cracks extending at least half the lane width (1.83 meters [6 feet] or longer cracks) to estimate the total length of cracking in terms of feet per mile (or meters per kilometer) normalized by the total length of the manual evaluation zone. In order to simulate the transverse cracking measurement, any transverse cracks longer than 1.83 meters (6 feet) were digitized in a GIS as polylines to facilitate the calculation of the total length of transverse cracking (Figure 6). The same polygon created in alligator cracking measurement representing the whole pavement section was used to measure the total length of the evaluation zone.

3.6 Measurement Result Comparison

Rutting depth, alligator cracking area percent, and transverse cracking length measured from the DSMs and orthophotos were compared to manual evaluation results to examine the feasibility of using the H-DAP derived outputs to detect and assess the pavement surface distress metrics. Linear regression analyses revealed that the H-DAP derived measurement and the manual measurement for all three

distresses fit closely to the regression lines. Therefore, a paired-t test was not performed to examine if the H-DAP derived measurement and the manual measurement are statistically different from each because these data clearly violate the assumption that there is no linearity between the two groups of sample values (Carroll and Ruppert 1996). Pavement surface distresses measured from these two methods were compared with orthogonal regression analysis because it does not assume independence between variables. Orthogonal regression examines the linear relationship between two continuous variables and is often used to test whether two instruments or methods are measuring the same thing (Staiger and Stock 1997). For both linear regression and orthogonal regression, the dependent variable is the reference distress rate measured by manual method. This also makes the usage of orthogonal regression appropriate because unlike linear regression, both the independent and dependent variables in orthogonal regression contain measurement error (Carroll and Ruppert 1996).

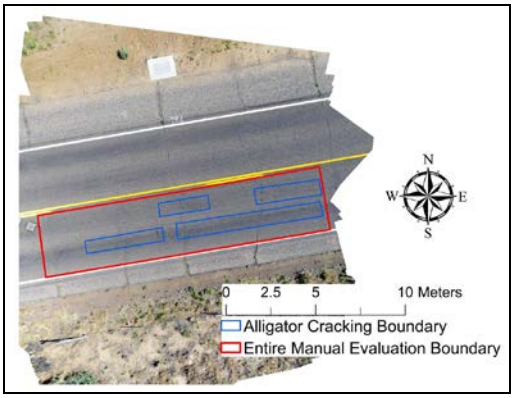

Figure 5: Alligator cracking boundary within entire manual evaluation boundary; blue polygons are the alligator cracking area while the red polygon is the entire manual evaluation zone; areas for these polygons can be calculated within the geographic information systems (GIS) and therefore, alligator cracking area percentage can be determined.

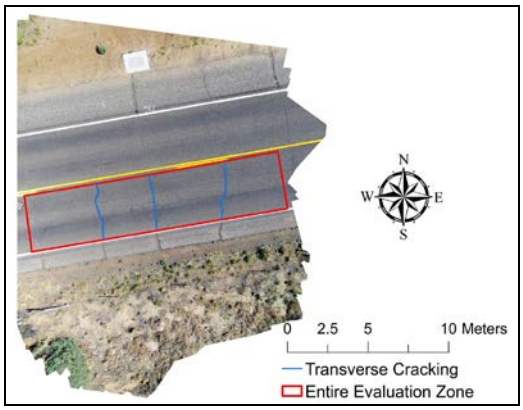

Figure 6: Transverse cracking and entire manual evaluation polygon boundary; the red polygon is the entire manual evaluation zone, while the blue polylines are the transverse cracks; lengths of these transverse cracks and the length of the manual evaluation zone can be calculated within the GIS and therefore, transverse cracking length normalized by the total evaluation zone length can be calculated.

4 RESULTS AND DISCUSSION

The manually-evaluated and H-DAP derived rutting depths are summarized and exhibited. It should be noted that the results are organized by inner and outer wheel paths for each data collection site (See Table 2 for details). Table 3 summarizes the manually-evaluated and H-DAP derived alligator cracking area percent and transverse cracking length.

Table 2: Manually-evaluated and DSM Derived Rutting Depth

Site ID	Inner Wheel Path (in meters)				Outer Wheel Path (in meters)			
	Measure Point	Manual Depth (1)	DSM Depth (2)	Error (1-2)	Measure Point	Manual Depth (3)	DSM Depth (4)	Error (3-4)
Site 1	1	0.022	0.025	-0.003	1	0.007	0.006	0.001
	2	0.020	0.022	-0.002	2	0.005	0.003	0.002
	3	0.020	0.024	-0.004	3	0.005	0.007	-0.002
Site 2	1	0.017	0.018	-0.001	1	0.010	0.005	0.005
	2	0.020	0.019	0.001	2	0.010	0.009	0.001
	3	0.025	0.023	0.002	3	0.008	0.005	0.003
Site 3	1	0.015	0.016	-0.001	1	0.010	0.009	0.001
	2	0.014	0.015	-0.001	2	0.005	0.007	-0.002
	3	0.016	0.017	-0.001	3	0.005	0.006	-0.001
Site 4	1	0.015	0.016	-0.001	1	0.011	0.012	-0.001
	2	0.020	0.019	0.001	2	0.005	0.004	0.001
	3	0.015	0.016	-0.001	3	0.011	0.010	0.001
Site 5	1	0.020	0.019	0.001	1	0.015	0.013	0.002
	2	0.020	0.019	0.001	2	0.011	0.013	-0.002
	3	0.020	0.018	0.002	3	0.020	0.018	0.002
Site 6	1	0.011	0.013	-0.002	1	0.016	0.018	-0.002
	2	0.012	0.011	0.001	2	0.018	0.019	-0.001
	3	0.020	0.024	-0.004	3	0.011	0.013	-0.002
Site 7	1	0.018	0.020	-0.002	1	0.025	0.026	-0.001
	2	0.022	0.024	-0.002	2	0.020	0.021	-0.001
	3	0.025	0.022	0.003	3	0.020	0.023	-0.003
Site 8	1	0.018	0.020	-0.002	1	0.015	0.016	-0.001
	2	0.020	0.021	-0.001	2	0.015	0.012	0.003
	3	0.010	0.012	-0.002	3	0.025	0.024	0.001
Site 9	1	0.015	0.014	0.001	1	0.020	0.023	-0.003
	2	0.015	0.013	0.002	2	0.016	0.015	0.001
	3	0.010	0.013	-0.003	3	0.012	0.015	-0.003
Site	1	0.005	0.008	-0.003	1	0.015	0.014	0.001
	2	0.010	0.013	-0.003	2	0.015	0.017	-0.002
	3	0.010	0.008	0.002	3	0.015	0.017	-0.002

Table 3: Manually-evaluated and Orthophoto-derived Alligator and Transverse Cracking Measurement

Site ID	Alligator Cracking Area (Percent)				Transverse Cracking (Feet/Mile)	
	Manual Evaluation		Orthophoto Evaluation		Manual Evaluation	Orthophoto Evaluation
	Actual	Rounded	Actual	Rounded		
Site 1	7.79	10	8.08	10	3336	3400
Site 2	3.36	5	4.71	5	3844	3968
Site 3	6.99	10	7.4	10	3200	3282
Site 4	13.99	15	12.51	15	6999	7185
Site 5	7.36	10	8.45	10	7366	7492
Site 6	24.95	25	22.43	25	5450	5518
Site 7	20.99	25	23.15	25	4088	4183
Site 8	18.46	20	19.16	20	5879	5923
Site 9	13.98	15	11.29	15	6000	6013
Site 10	24.88	25	27.49	30	3450	3579

Table 4 shows the linear and orthogonal regression results for all three types of distresses. In this table, Coef indicates coefficient; SE indicates Standard Error; and CI indicates confidence interval. For all three types of distresses, linear regression results revealed that the distress rates measured by manual methods and H-DAP method correlated well (rutting $R^2 > 0.92$; alligator cracking $R^2 > 0.96$, and transverse cracking $R^2 > 0.99$). Therefore, instead of using a paired-test, orthogonal regression analysis was used in this study because it does not assume independence between variables. Interpretation of the

orthogonal regression results should be focused on the CI. It indicates that the measurements from the manual method and H-DAP method are not statistically different if zero is contained in the CI for the intercept and one is contained in the CI for the slope. Results revealed that there is no evidence showing that distress rates measured by manual method and H-DAP method are statistically different.

Table 4: Linear Regression and Orthogonal Regression Results

Distress	Regression	Independent Variables	Coef	P Value	95% CI	R^2
Rutting	Linear	Intercept	-0.00004	0.934	(-0.0012387, 0.00114)	0.9255
		DSM Depth	0.96850	<0.0001	(0.8962828, 1.040724)	
	Orthogonal	Intercept	-0.00065	0.290	(-0.001859, 0.00056)	N/A
		DSM Depth	1.00770	<0.0001	(0.934107, 1.08128)	
Alligator Cracking	Linear	Intercept	1.34855	0.221	(-0.99231, 3.689406)	0.9695
		Orthophoto Area Percent	0.88797	<0.0001	(0.75959, 1.016341)	
	Orthogonal	Intercept	1.14033	0.267	(-0.87417, 3.15483)	N/A
		Orthophoto Area Percent	0.90059	<0.0001	(0.78988,1.01129)	
Transverse Cracking	Linear	Intercept	-64.46947	0.299	(-198.2345, 69.29554)	0.9990
		Orthophoto Length	0.9943354	<0.0001	(0.96896, 1.01971)	
	Orthogonal	Intercept	-66.94152	0.249	(-180.688, 46.8046)	N/A
		Orthophoto Length	0.99482	<0.0001	(0.973, 1.0164)	

Ultimately, these results show that H-DAP method works as effectively as the manual evaluation does. Given the horizontal and vertical accuracy of the DSMs and orthophotos, the discrepancy between manual method measurement and the H-DAP method measurement could be from either method. Distresses measured by different inspectors have been shown to exhibit a high degree of variability (Bogus et al. 2010) because this method relies on subjective visual observation, suggesting that manual assessments will naturally exhibit variability. These results can be interpreted to indicate that H-DAP based method is at least as accurate as manual methods.

5 CONCLUSIONS

We present a novel approach for detailed infrastructure condition assessment using H-DAP acquired from a low-altitude URSS. Using roadway pavement assets as an example, results indicate that pavement surface distress conditions measured by manual methods and the H-DAP method are not statistically different from each other and that the proposed method is likely more accurate than manual methods. In the near-term, the proposed H-DAP method could be used to measure infrastructure conditions in situations where field inspectors cannot evaluate except with considerable labor costs (e.g. sections in remote areas) or where vehicles cannot access, but in the longer-term, the proposed method is capable of completely replacing field infrastructure condition assessment due to its high accuracy, potential for full automation, and dramatically reduced long term cost.

Acknowledgements

This study has been funded by the Research Allocations Committee of the University of New Mexico. This study has also been supported by National Science Foundation (award # CMMI-1360041) and the U.S. Department of Transportation (cooperative agreement # OASRTRS-14-H-UNM). The views, opinions, findings and conclusions reflected in this presentation are the responsibility of the authors only and do not represent the official policy or position of the USDOT/OST-R, or any State or other entity.

References

Aber, J., Sobieski, R., Distler, D. and Nowak, M. 1999. Kite Aerial Photography for Environmental Site Investigations in Kansas. *Transactions of the Kansas Academy of Science,* **102** (1-2): 57-67.
Aber, J., Aber, S.W. and Leffler, B. 2001. Challenge of Infrared Kite Aerial Photography. Transaction of the Kansas Academy of Science, **104**(1-2): 18-27.
Aktan, A.E., Farhey, D.N., Brown, D.L., Dalal, V., Helmicki, V.J., Hunt, V.J. and Shelley, S.J. 1996. Condition Assessment for Bridge Management. *Journal of Infrastructure Systems,* **2**(3): 108-117.
Bogus, S.M., Song, J., Waggerman, R. and Lenke, L. 2010. Rank Correlation Method for Evaluating Manual Pavement Distress Data Variability. *Journal of Infrastructure Systems*, **16**(1): 66-72.
Carroll, R.J. and Ruppert D. 1996. The Use and Misuse of Orthogonal Regression in Linear Errors-in-Variables Models. *The American Statisticians*, **50**(1): 1-6.
Chen, S., Rice, C., Boyle, C., and Hauser, E. 2011. Small-format Aerial Photography for Highway-bridge Monitoring. *Journal of Performance of Constructed Facilities,* **25**(2): 105-112.
Cordova, A.A., Bogus, S.M., Migliaccio, G.C. and Lenke, L.R. 2009. *2009 Pavement Evaluation Report: Northern New Mexico.* Department of Civil Engineering, University of New Mexico, Albuquerque, NM.
Fraser, W., Carlson, J., Duley, P., Holm, E. and Patterson, D. 1999. Using Kite-based Aerial Photography for Conducting Adelie Penguin Censuses in Antarctica. *Waterbirds: The International Journal of Waterbird Biology,* **22**(3), 435-440.
Guichard, F., Bourget, E. and Agnard, J. 2000. High-resolution Remote Sensing of Intertidal Ecosystems: A Low-cost Technique to Link Scale-dependent Patterns and Processes. *Limnology and Oceanography,* **45**(2): 328-338.
Guo, H.D. 2010. Understanding Global Natural Disasters and the Role of Earth Observation. *International Journal of Digital Earth,* **3**(3): 221-230.
Highway Performance Monitoring System Field Manual. 2010. Office of Highway Policy Information, Federal Highway Administration, U.S. Department of Transportation.
Hudson. W.R. and Uddin, W. 1987. Future Pavement Evaluation Technologies: Prospects and Opportunities. 2nd North American Pavement Management Conference, Toronto, Canada, 233-258.
Jensen, J.R. and Cowen, D.D. 1999. Remote Sensing of Urban/Suburban Infrastructure and Socio-Economic Attributes. *Photogrammetric Engineering and Remote Sensing*, **65** (5): 611-622.
Karaa, F.A. 1989. Infrastructure Maintenance Management System Development. *Journal of Professional Issues in Engineering Education and Practice,* ASCE, **115**(4): 422-432.
Marzolff, I. and Poesen, J. 2009. The Potential of 3D Gully Monitoring with GIS Using High-resolution Aerial Photography and a Digital Photogrammetry System. Geomorphology, **111**(1-2): 48-60.
Maser, K. 1988. Inventory, Condition, and Performance Assessment in Infrastructure Facilities Management. *Professional Issues in Engineering Education and Practice,* ASCE, **114**(3): 271-275.
Maser, K. 2005. Automated Systems for Infrastructure Condition Assessment. *Journal of Infrastructure Systems,* ASCE*,* **11**(3): 153-153.
Scoffin, T. 1982. Reef Aerial Photography from a Kite. *Journal of Coral Reefs,* **1**(1): 67-69.
Sklaver, B., Manangan, A., Bullard, S., Svanberg, A. and Handzel, T. 2006. Rapid Imagery through Kite Aerial Photography in a Complex Humanitarian Emergency. *International Journal of Remote Sensing,* **27**(21-22):4709-4714.
Smith, M., Chandler, J. and Rose, J. 2009. High Spatial Resolution Data Acquisition for the Geosciences: Kite Aerial Photography. *Earth Surface Processes and Landforms,* **34**(1): 155-161.
Staiger, D. and Stock, J.H. 1997. Instrumental Variables Regression with Weak Instruments. *Econometrica*, **65(**3): 557-586.
Verhoeven, G. 2009. Providing an Archaeological Bird's-eye View – an Overall Picture of Ground-based Means to Execute Low-altitude Aerial Photography in Archaeology. *Archaeological Prospection,* **16**(4), 233-249.
Wundram, D. and Loffler, J. (2008). High-resolution Spatial Analysis of Mountain Landscapes using a Low-altitude Remote Sensing Approach. *International Journal of Remote Sensing*, **29**(4): 961-974.
Zhang, S. and Bogus, S. 2014. Use of Low-cost Remote Sensing for Infrastructure Management. Construction Research Congress, ASCE, Atlanta, GA, USA, 1299-1308.
Zhang, Y., Xiong, J. and Hao, L. 2011. Photogrammetric Processing of Low Altitude Images Acquired by Unpiloted Aerial Vehicles. *The Photogrammetric Record,* **26**(34): 190-211.
Zomrawi, H., Hussien, M.A. and Mohamed, H. 2013. Accuracy Evaluation of Digital Aerial Triangulation. *International Journal of Engineering and Innovative Technology*, **2**(10): 7-11.